Available online at www.sciencedirect.com
ScienceDirect
Journal of Solid State Chemistry 180 (2007) 885–893
JOURNAL OF SOLID STATE CHEMISTRY
www.elsevier.com/locate/jssc

TEM investigation of the microporous compound VSB-1: Building units and crystal growth mechanisms

Marie Colmont*, Osamu Terasaki

Structural Chemistry, Arrhenius Laboratory, Stockholm University, S-10691 Stockholm, Sweden

Received 25 August 2006; received in revised form 17 November 2006; accepted 12 December 2006
Available online 27 December 2006

Abstract

Surface fine structure and structural defects in the open framework material VSB-1 have been investigated by electron microscopy. Crystal growth phenomena are proposed by a building unit model: (i) a unit is formed by two building units; (ii) they are linked to form first channels; and (iii) the whole network is grown via a layer-by-layer growth mechanism. A planar defect was observed in high-resolution transmission electron microscope (HRTEM) image taken with the [0001] incidence, and diffuse streaks related to the presence of defects were observed in a series of electron diffraction (ED) patterns. The microstructure model derived from the defect structure gives information on crystal growth. These defects highlight an open site that could be the pillar of a new crystal growth process. The study of defects and crystal growth is important in understanding physical properties such as catalytic or magnetic properties, and in synthesising a new open framework structure.

Keywords: Microporous material; Electron microscopy; Crystal growth

1. Introduction

Porous materials are classified according to the sizes of their pores. If the pore size is larger than 500 Å, the compounds are named macroporous. Solids with a pore size in the range of 20–500 Å are mesoporous materials, and if the pore size is below 20 Å, they are called microporous materials on which we will focus in this paper.

Microporous materials include different subgroups of compounds such as Zeolites [1,2], Metal Oxide Frameworks [3], hybrid inorganic–organic materials [4], Chalcogenides [5,6], Nitrides [7], Halides [8], etc. The differences between them are related to the nature of the major component of the framework, i.e., a building block, based upon as many as 25 elements of the periodic table. The study of microporous frameworks has become a subject of great interest, and numerous ideal framework types have now been determined and catalogued. Understanding what are the growth units, how crystals nucleate and grow, how order is created from disorganisation and what drives this, is important to discover and synthesise new related phases.

These microporous materials have been studied intensively during the last decade because of their potential applications in diverse areas such as gas separation, ionic exchangers, photo luminescence and catalysis. The catalytic activity is closely related to high surface areas with suitable catalytic centres. Selectivity is linked to the shape of the pores [9]. For this reason, scientists are searching for new materials with different pores in shape and size to reach further applications. This can be guided by an understanding of the building units, the crystal growth mechanisms and the exterior surface fine structures. Structural defects influence on the catalytic activities. In the case of open framework structures, the types of defects are as diverse as the number of structures that can be formed, for example: metal-substituted sites, intergrowths, faults, and hydroxide nests, making their structural characterisation complicated. By defects we mean any part of the structure that deviates from the regular pattern of the ordered 3D crystal structure. Even in very small concentrations, framework defects locally reshape the pore

*Corresponding author. Fax: +33 3 20 43 68 14.
E-mail address: marie.Colmont@ensc-lille.fr (M. Colmont).

0022-4596/$ - see front matter © 2007 Elsevier Inc. All rights reserved.
doi:10.1016/j.jssc.2006.12.018

structure, creating a variety of new potentially active sites that may significantly change the common properties. The types of defects that are incorporated into a framework-type structure are often a consequence of the crystal growth process itself. So explaining catalytic properties requires an understanding of both crystal structure and defects. In this paper, we will study this growth process and the defects that occur in the microporous VSB-1 compound using HRTEM [10,11].

Crystal growth and defects are local phenomena in the structure and must be therefore studied with methods that provide detailed information of not average but local structure. Transmission electron microscopy (TEM) is ideally suited to this. HRTEM is a powerful technique to elucidate the external surface structure, which has already been observed for zeolites [12–15], and to study defects. The obtained information can be used to establish a model of crystal growth and to evaluate different possible crystal growth mechanisms.

TEM has been used to investigate the large pore zeolitic nickel(II) phosphate, VSB-1, evidenced by Guillou et al. [16]. This interesting porous material has been largely studied for its magnetic and catalytic properties [14,17–19] and its capacity to store hydrogen [20]. In this case, once you manage to pass over the difficulties of studying such beam-sensitive material, the use of TEM helps to obtain explanation on the structure itself and on the mechanisms of crystal growth, through the observation of diffuse streaks on ED patterns and defects on HREM images, both of them are closely related to each other.

2. Experimental section

Synthesis of the microporous compound VSB-1 was done following the procedure of Guillou et al. [16]. A mixture of nickel(II) chloride hexahydrate, phosphoric acid (85% by weight), tris(2-aminoethyl)amine (TREN), pyridine, hydrofluoric acid (40% by weight) and water as a solvent (molar ratios: 5:5:2:9:12:200) was placed in an autoclave at 453 K during 6 days. A Teflon beaker was used to prevent reaction with the vessel. After the hydrothermal reaction, the green pistachio precipitate was washed with deionised water and the product was dried to remove adsorbed water at 120 °C in air. The purity of the sample was checked by powder X-ray diffraction (XRD). XRD patterns were recorded on an STOE powder diffractometer equipped with Cu $K\alpha$ radiation (40 kV, 20 mA) at a rate of $1.0^\circ\,min^{-1}$ over the range of 1.0–20.0° in scattering angle.

TEM observation was carried out with a JEOL JEM-3010 microscope operating at 300 kV ($C_s = 0.6$ mm, resolution 1.7 Å). Images were recorded with a CCD camera (model Keen View, SIS analysis, 1024×1024 pixels, pixel size 23.5×23.5 μm). The sample was crushed for half an hour in an agate mortar to prevent effects from preferred orientation and crystal morphology, dispersed in ethanol by ultrasonic method, and deposited on a holey carbon microgrid. Electron diffraction (ED) patterns were used to check the presence of new phases and also to confirm the unit cell parameters of VSB-1. Au particles were spattered onto the carbon grid as an internal standard in order to calibrate the camera length. After calibrating the camera length from the Debye ring from the gold particles, it was confirmed that the specimen was a single phase, and the unit cell parameters were refined as $a = 19.87(5)$ Å, and $c = 5.05(4)$ Å. These values are in good agreement with the data ($a = 19.834(1)$ Å, and $c = 5.0379(8)$ Å) mentioned in Ref. [15] and refined from XRD study.

The crystal size and morphology of the material were studied in a scanning electron microscope SEM, JEOL 820.

3. Structure reminder

The complex structure of VSB-1 led to the determination of an average structure, leaving the finer details still

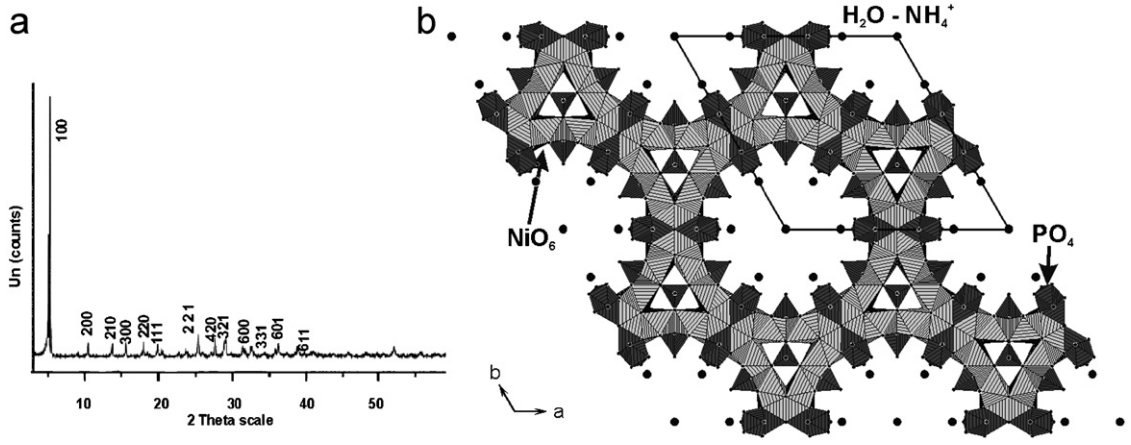

Fig. 1. (a) XRD pattern of VSB-1 showing preferred orientation of (100); and (b) projection of the two-dimensional structure: VSB-1. NiO_6 polyhedra are shown in light grey while PO_4 tetrahedra are in dark grey. Inside the channels, NH_4^+ and H_2O molecules are represented by black circles.

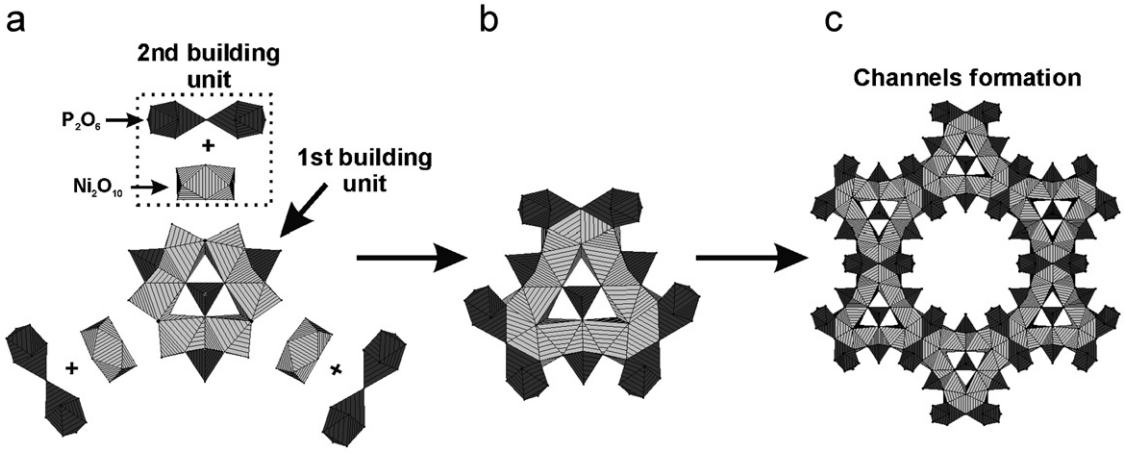

Fig. 2. The two building units of the structure represented along the [0001] direction. (a) The first one consists of six edge-sharing NiO_6 octahedra and four PO_4 groups. The second one is an association of disordered PO_4 and NiO_6 groups. (b) These building units are connected together to form the channels (c).

unknown [15]. VSB-1 crystallises in the hexagonal system, space group *P6mm*, with the following unit cell parameters: $a = 19.834(1)$ Å, and $c = 5.0379(8)$ Å. Fig. 1 shows the XRD pattern of VSB-1 and a representation of the structure along the *c*-axis. The association of NiO_6 octahedra sharing edges and corners leads to the formation of channels. PO_4 tetrahedra are linked to the surface of those channels and are also situated at the centre of a six-ring of NiO_6 octahedra. This structure contains two building units as shown in Fig. 2(a). The first one consists of a six edge-sharing NiO_6 octahedra and four PO_4 tetrahedra of which one of them takes place at the centre of the six-ring NiO_6 octahedra. The second building unit is an association of two disordered PO_4 tetrahedra and NiO_6 octahedra. In Ref. [15], this is mentioned as one independent unit, but we prefer to refer separately to the PO_4 and NiO_6 parts of the building unit. The second building units come in addition to the first ones (Fig. 2(b)) and are linked together to form one-dimensional 24 member ring channels (Fig. 2(c)). This leads to a two-dimensional hexagonal network of channels inside which are localised ammonium and water molecules. In the case of such a difficult refinement and complicated structure, TEM plays an important role and can complete the XRD study.

4. Result and discussion

4.1. Difficulty of microscopic study

The TEM study of such materials, sensitive to the electron beam, is very difficult. Very few TEM studies of metal phosphate have been achieved and, they usually show results on ED study only [21]. From this point of view, the study of VSB-1 is difficult and needs special care. Indeed, under conditions of common TEM observation, the structure collapses after a few minutes of irradiation. To avoid this phenomenon, the intensity of incident electron has been reduced by both enlarging the incident beam and using a small condenser aperture (minimum flux and part of electron). HREM images were taken at low magnification and in under-focus conditions (to enhance the contrast of the pores).

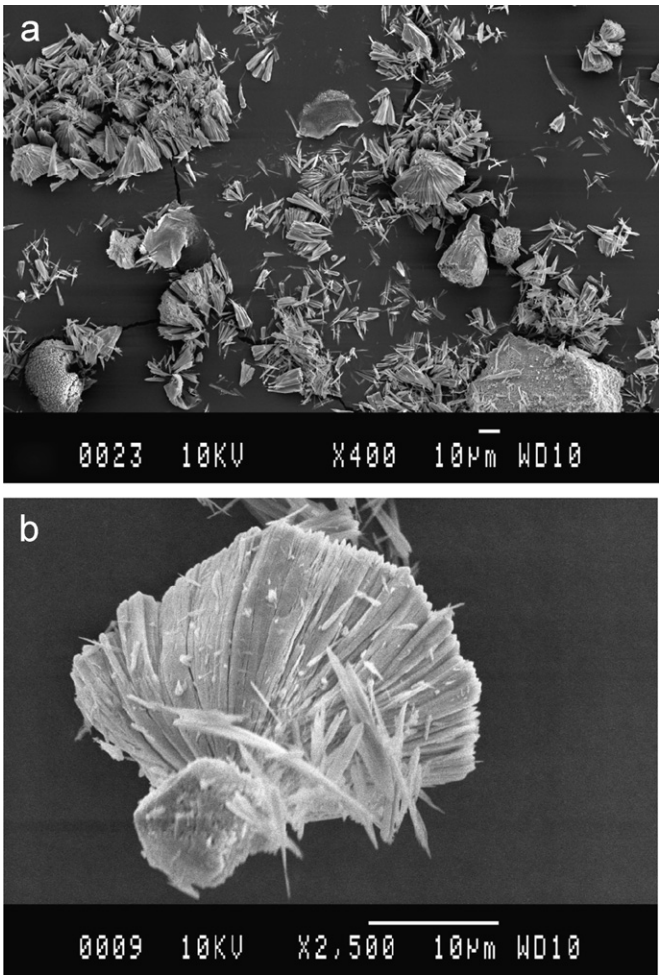

Fig. 3. Particle morphologies observed using Scanning Electron Microscopy: (a) low magnification and (b) high magnification.

The crystal morphology of crystallites was also a bad point to overcome. VSB-1 crystals have a sharp needle-shaped morphology (see scanning electron microscopy (SEM) image in Fig. 3). Almost all particles form aggregates. Crystals grow along the *c*-axis (the axis of channels), creating a preferred orientation. This phenomenon, already observed in XRD patterns (intensity of (100), is huge compared with (001)), and made the observation along the [0001] direction particularly difficult. This problem was overcome by crushing the sample over a large period to break up the needles.

4.2. Evidence of defects

4.2.1. Electron diffraction study

Selected area electron diffraction (SAED) patterns and HRTEM images were recorded along [0001] (Fig. 4(a) and (c)) and [10-10] (Fig. 4(b) and (d)) directions. Observed spots are very sharp, highlighting the high crystallinity of the sample (already evidenced by an XRD observation). The reflections of these two principal planes can be indexed in a primitive hexagonal unit cell with the same parameters as those determined from the XRD data. Any extinction condition is evidenced by reinforcing the *P6mm* space group. HRTEM images taken along the two identical directions are indicative of a structure with a honeycomb array of one-dimensional pores. Fig. 4(c) and (d) show pores, respectively, parallel and perpendicular to the incident electron beam.

A series of ED patterns were observed from several crystallites. Diffuse streaks parallel to b^* and localised between fundamental Bragg reflections were observed in ED patterns taken with $[20-2n]$, $n =$ odd, incidences for all crystallites. They are highlighted by white arrowheads in Fig. 5(a)–(c) for [20-21], [20-23] and [20-25] incidences, respectively. The presence of diffuse streaks is not surprising as diffuse scattering has already been observed by the authors on X-ray photos taken at Daresbury [15]. Optical densitometer scans of the diffuse scattering along b^* reveals a continuous intensity distribution along b^*. In

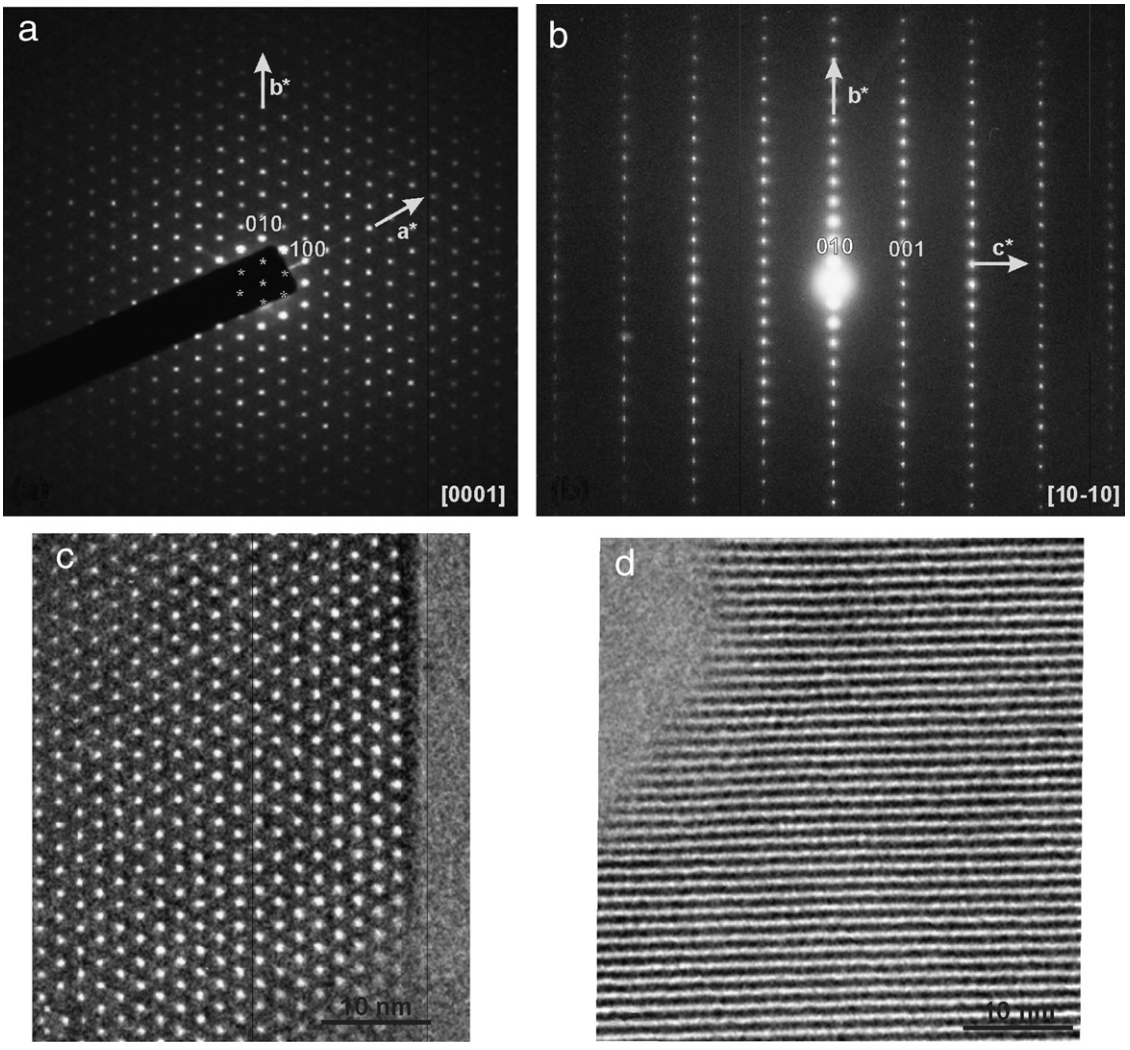

Fig. 4. ED patterns of VSB-1 taken along the (a) [0001] and (b) [10-10] direction. HRTEM images recorded along the same high-symmetry axes showing pores parallel (c) and perpendicular (d) to the electron beam. Differences in *d*-spacing along a^* and b^* (010 and 100) is due to the scale of images.

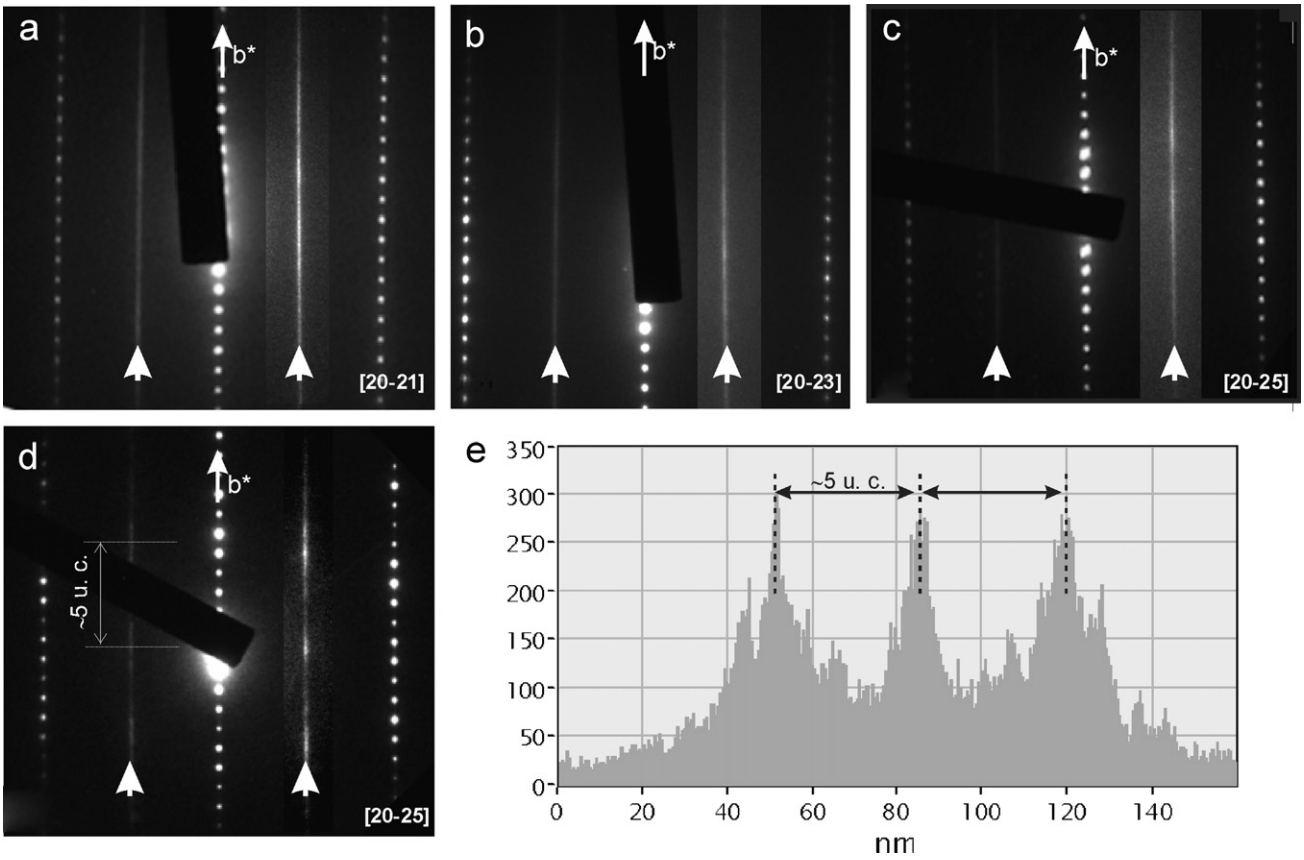

Fig. 5. Experimental (a) [20-21], (b) [20-23] and (c) [20-25] ED patterns showing diffuse streaks parallel to b^*. In each ED pattern, a contrast of a strip containing diffuse streaks on the right-hand side relative to the origin is adjusted to enhance diffuse streaks. Sometimes, a modulation of the intensity of streaks occurs with a periodicity of five unit cells as shown on (d) and (e). Differences in d-spacing along b^* is due to the scale of images.

some cases, we noticed an intensity modulation of streaks as pointed out in Fig. 5(d) and (e). We observe diffuse streaks for [20n], where n = odd incidences, so the diffuse intensities are distributed as a series of lines running parallel to the b^*. The presence of these diffuse streaks is slightly related to the short-range order, meaning a phenomena occurs at the range of the building units.

4.2.2. Images study

To complete this study, an HRTEM image was taken along [20-25] (Fig. 6(a)). The same streaks parallel to b^* were observed on the FFT (Fast Fourier Transform) of this image (Fig. 6(b)). A mask selecting the central spot and the diffuse streaks was applied on the FFT. Before all discussion, we should note that the same mask, when applied to an empty image, gave sharp lines inclined to b by ca. 45°: they are generated by the square mask used for producing the FFT pattern. So the streaks parallel to b^* are totally generated by the crystal defects themselves. Then, by inverse FFT, we localized the effects of these streaks on the real image (Fig. 6(d)). The inverse FFT is made by wavy fringes and, perpendicularly to them, by lines of different contrasts. In the reciprocal space, the distance between b^* and diffuse streaks is equivalent to the distance between four black fringes, and each one is separated by a white fringe. This is highlighted by a star in the inset in Fig. 6(d). The streak itself generates the lines perpendicular to b^*. The distance between these lines varies randomly. It means that the extra phenomenon occurring there has a variable periodicity as mentioned before (between 4-and 6-unit cells). Combining this idea with the average structure obtained by the authors, this phenomenon can be explained as follows. Along a [20−2n], n = odd, axis, the structure consists partly of layers of the disordered NiO_6 octahedra and PO_4 tetrahedra of the second building unit mentioned in Fig. 2. This is in good agreement with (i) the position of diffuse streaks on ED patterns and (ii) the localisation of the effect of streaks on the inverse FFT. Especially the presence of the Ni_2 site, partially occupied by Ni atoms, goes with such disordered phenomenon. The streak itself includes two phenomena: either a difference of atom type, precisely between nickel and phosphorus atoms in our case, or the atomic position. The nature of atoms is related to the atomic scattering factor and modifies the amplitude of the streaks, whereas the atomic position is related to the phase effect. These atoms were previously refined by powder XRD (Ref. [16]) profile analysis with half occupancy rates suggesting the presence of disorder in this part of the unit cell. Nickel and phosphorus atoms alternates with different occupancy rates and their atomic positions can be slightly shifted, perpendicularly to b^*, around the average position refined

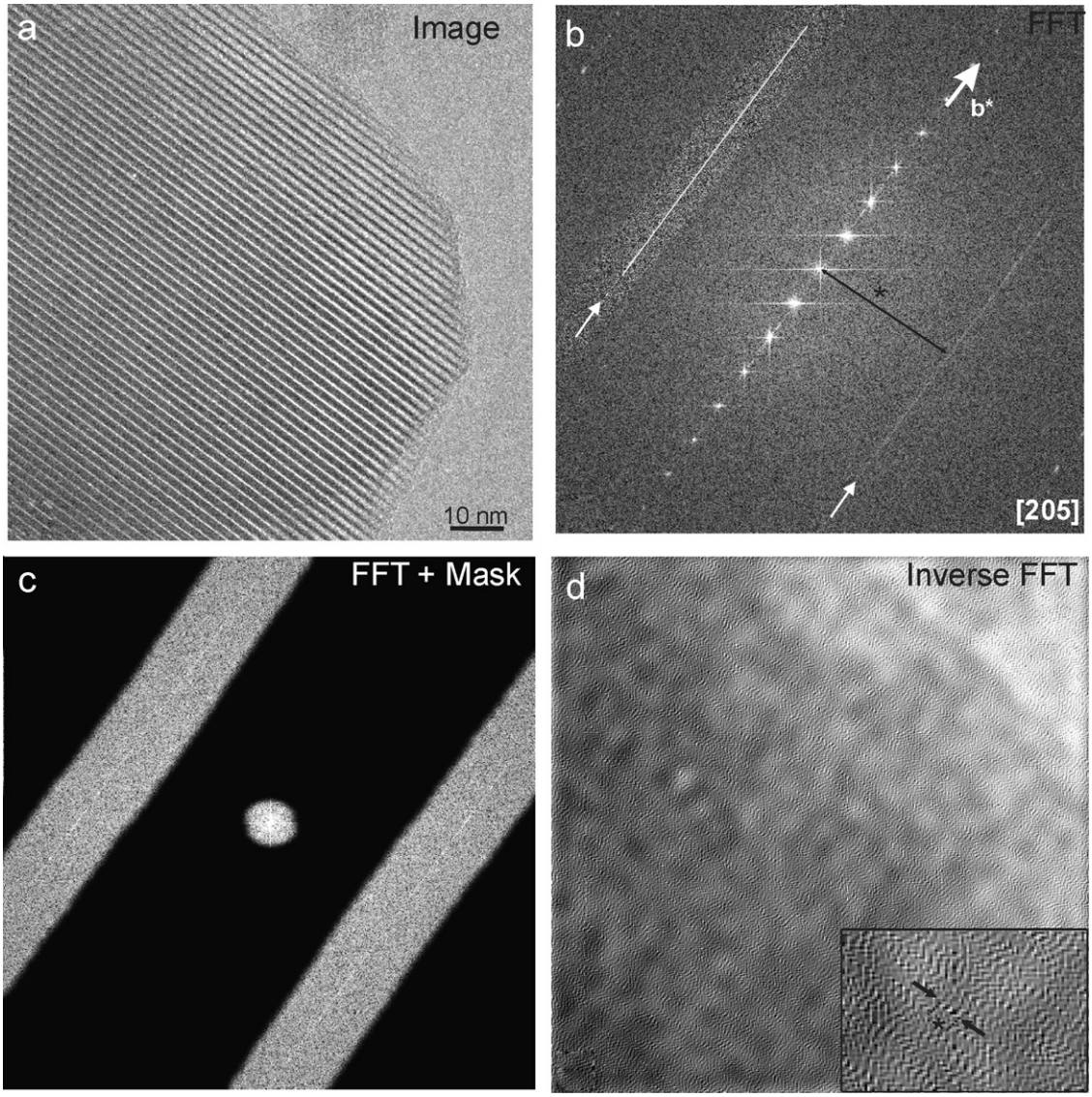

Fig. 6. (a) HRTEM image of VSB-1 taken along [20-25], (b) FFT obtained from the thinnest part of this image, showing the fundamental Bragg reflections and diffuse streaks parallel to b^*, (c) a mask was applied on the FFT to select the contributions of the central spot and the diffuse streaks. The inverse FFT of it allowed determination of the contribution of diffuse streaks on the initial image (d). The corresponding distance between the central spot on the FFT, in the reciprocal space (b), is evidenced in the real space by a star (d).

from XRD data by the authors. Nevertheless, the modulation of diffuse streaks intensity presented in Fig. 6(e) goes with a tendency of some ordering each five unit cells, meaning a periodic arrangement between the two types of atoms. These reasons can explain the relatively low intensity of streaks observed on the FFT. The capacity of nickel and phosphorus atoms to adapt themselves to a closed environment is quite important, as will be shown in the next part. They make the building units flexible to adapt to new environments.

5. Defect analysis: crystal growth study

Images taken along [0001] reveal the presence of defects as shown in Fig. 7(a). Thermodynamically speaking, all crystals contain defects, but for open framework structures, the type of defects tends to be especially very large and as varied as the nature of different structures that can be formed. The crystal growth process is often severely modified by the incorporation of such defects. So, structural characterisation of them is the key to understand the crystal growth process of this structure. HRTEM is an important tool for studying defects in such open framework materials. Especially, it helps in three different ways to understand the crystallisation mechanism. First of all, HRTEM is perhaps the only technique used to study the surface termination structure of crystallites. We assume the surface fine structures were not damaged seriously during the preparation of the sample, especially by crushing. It can be noticed from Fig. 7(b) how half pores of the 24 member rings terminate the structure. Crystallites are terminated by (11-20) and (10-10) facets (Fig. 7(b) and (c)). This means

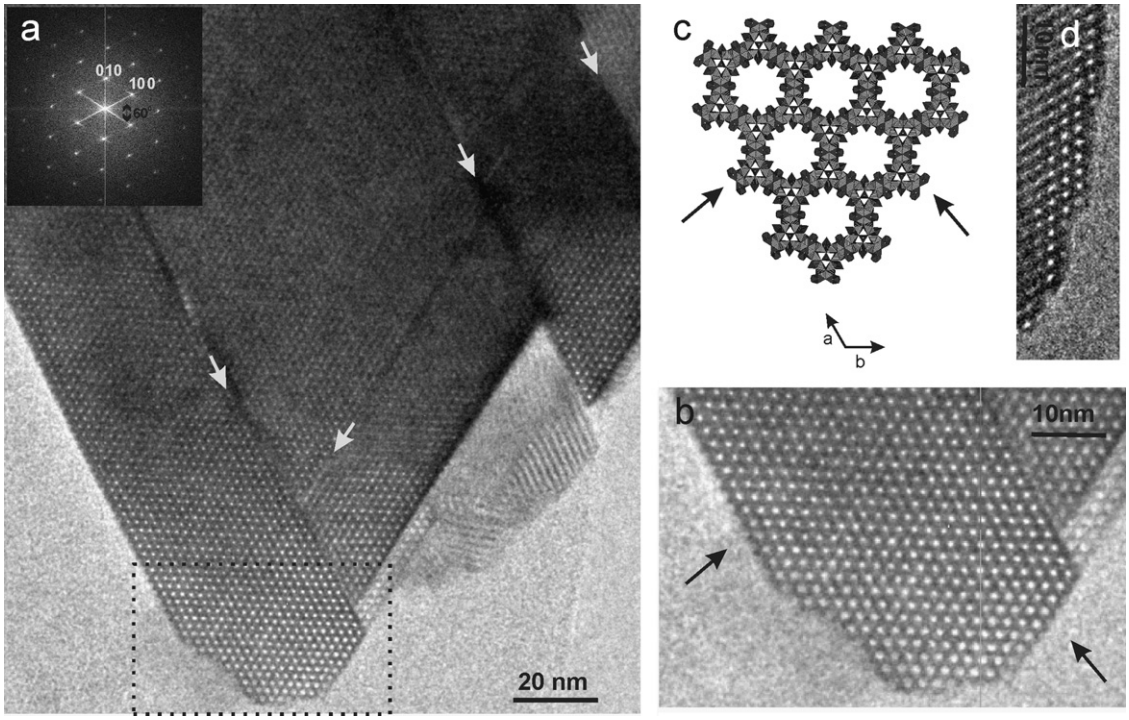

Fig. 7. (a) HRTEM image of VSB-1 viewed down *c*-axis (straight channels). Stacking faults defects are highlighted by white arrowheads. The corresponding FFT presented in insert shows diffuse streaks perpendicular to the defects and due to them. The selected area is enlarged on (b) to show the two typical surface terminations drawn on (c). (d) Terrace on surface.

that the internal void space in the structure is closed, and the only possibility to enter the channels is from [0001] direction. Knowing how crystallisation proceeds is important, particularly, in case of new materials growing on the surface structure itself. The different contrasts observed in several parts of the image (Fig. 7(a)) and also some surface shapes observed in Fig. 7(d) suggest the presence of surface terraces. The height of terraces corresponds to the size of one pore. Usually, atomic force microscopy is used to complete crystal structure analysis and, particularly, to reach fine details of the surface structure, for example, related to the morphology of terraces (precise height, circular, triangular shape, etc). Nevertheless, the size of crystallites is not big enough to use this method. These explanations about surface structure are in good agreement with a layer-by-layer growth mechanism in VSB-1, as it is mostly observed for open framework materials [8,9,22]. The two building units (Fig. 2(a) and (b)) are linked together to form the observed channels which stay open at the surface.

The second purpose of HRTEM is to understand intergrowth or twinning, [8,23] but neither of them has been observed during our study.

The third one is related to the structural analysis of defects, especially in terms of building unit structure. Their nature and concentration give information about crystal growth processes. The defect observed in Fig. 7(a) is commonly obtained with [0001] incidence. Fig. 8(a) shows it once more while capturing a clever view of the structure defect. These stacking faults are localised in several parts of crystallites and are growing along (10-10) and (11-20) as shown in Figs. 7(a) and 8(a). Fig. 8(b) is an enlargement of Fig. 8(a). From a structural model of this defect was established the drawing presented in Fig. 8(c). This defect comes from the association of two exactly identical networks of VSB-1 structure, translated relative to each other by ~0.40 nm along [1-10 0]. The distance between two parallel rows of channels in the defect structure is around 3.18 nm while it is normally equal to 1.69 nm in the structure of VSB-1. Keeping this in mind, the microstructure was modelled in the unit cell $a = 19.652$ Å, $b = 31.0000$ Å, $c = 5.018$ Å, $\alpha = \beta = \gamma$ 90°, space group $P1$. The predicted drawing is presented in Fig. 8(d). The two frameworks of channels are connected together by sharing a vertex of PO_4 tetrahedra of the first building unit and of NiO_6 octahedra of the second building unit, which is pointed out by black arrowheads in Fig. 8(d). It is worth noting that this second building unit is also responsible for the streaks previously observed. These two phenomena observed by different ways (ED patterns and HREM) are linked together and comes from the same origin: disorder in NiO_6 and PO_4, i.e. flexibility of the building units. The disordered unit already mentioned above plays an important role. The capacity of polyhedra to accommodate slight distortions in bond distances and angles allows the presence of such microstructures. It is worth noting that regarding the result mentioned, the distorted octahedra corresponds to the one surrounding Ni_2, which is a disordered site mentioned in Ref. [16]. In this case, it is better to differentiate between both parts of the second

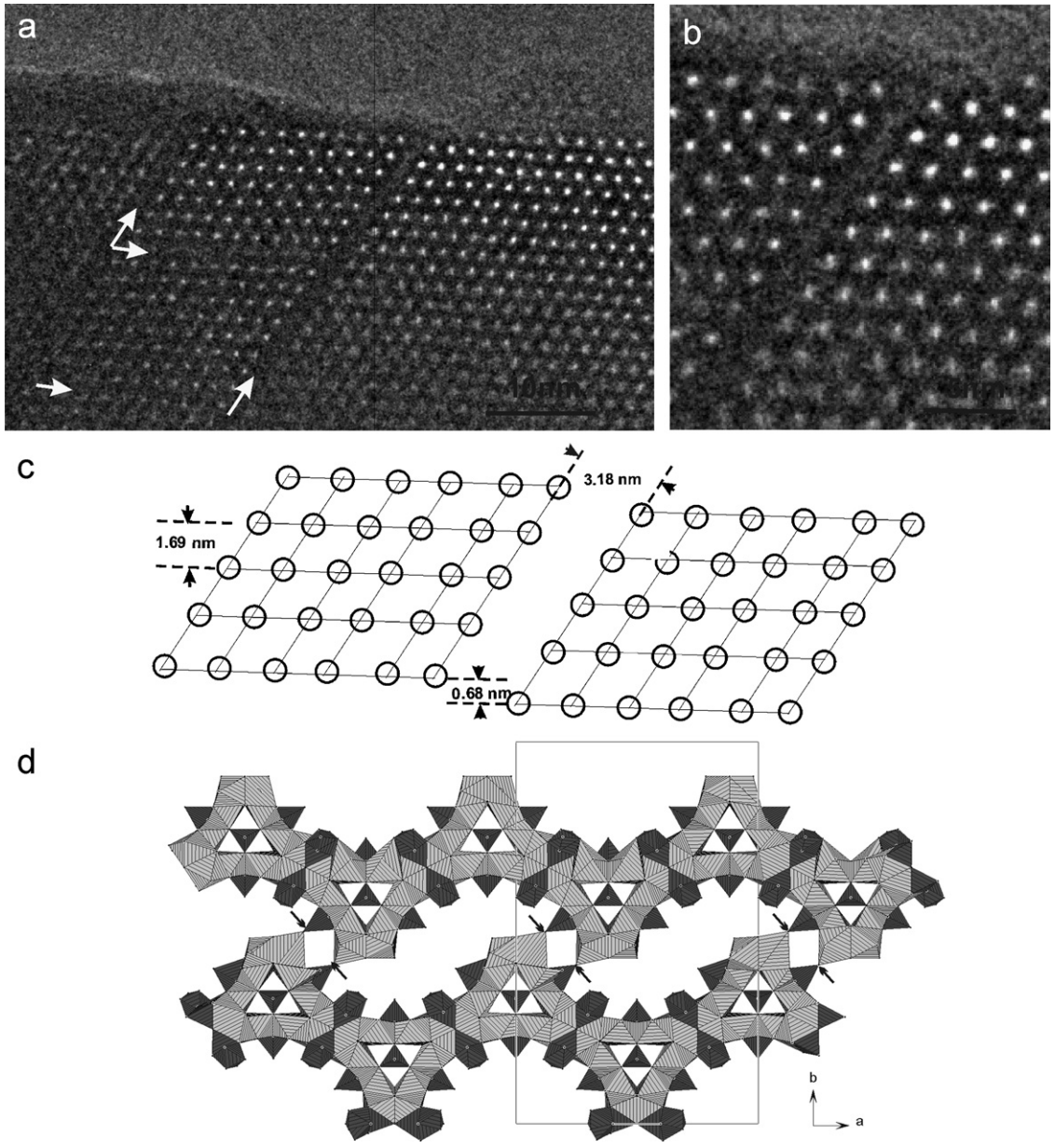

Fig. 8. (a) HRTEM image of VSB-1 viewed down *c*-axis (straight channels) and showing stacking faults evidenced by white arrowheads. (b) Enlargement of previous image enables the drawing of the microstructure (c). (d) Model of the microstructure obtained. The connection between the two identical networks is highlighted by black arrowheads.

building unit because the environment goes better with the presence of nickel octahedra only.

- First possibility: Keep the nickel atom in the same position. Then the distance between the central nickel atom and the surrounded oxygen atom shared with the phosphate group is elongated from 2.2 to 2.5 Å, which stays a valuable value for such polyhedra but generates much distorted polyhedra.
- Second possibility: The same scheme obtained with PO_4 tetrahedra is impossible as the tetrahedra would be too distorted, leading to an unbelievable configuration (greatly distorted tetrahedral with impossible P–O distances and O–P–O angles).
- Third possibility: The presence of fluorine in the structure is also important. Fluorine could replace oxygen around phosphorus and nickel, i.e., this site could preferably host fluorine than oxygen, allowing the growth of this defect? Certainly not because this is chemically not plausible, and the difference between P–F and Ni–F distances and P–O and Ni–O once is very small on the scale observed.
- Fourth possibility: Move nickel or phosphorus atom slightly from its central position to adapt to its new local environment and stay in possible octahedra. The displacement of this atom can be explained from diffuse streaks. As streaks are parallel to b^*, the displacement is perpendicular to the *b*-axis. This displacement tends to a

periodic arrangement in each five unit cell, as observed on some ED patterns. In this case, all Ni(P)–O distances are modified. To sum up, this microstructure comes certainly from the displacement of Ni or P atom to adapt to the oxygen and fluorine environment. The obtained microstructure consists of a four-member ring channel and a 22-member ring (20 NiO_6 octahedra and 2 PO_4 tetrahedra) with an oval shape.

The capacity of this part of the structure to adapt different structural environments is a key of crystal growth. These two nickel octahedra could be the root of new structures growing by connection with new building units. It is specially the flexibility of the building units discussed in the previous part that allows the formation of this microstructure. Fig. 7(a) evidences different periodicity of the microstructure. As it has a tendency to grow in each five unit cell, a future project could be to find a precise condition of synthesis allowing the formation of a new structure built on the microstructure inserted in the VSB-1 networking each five unit cell.

6. Conclusion

The presence of defects in VSB-1 open framework material has been studied by electron microscopy combining data from ED patterns and high-resolution electron microscopy images. As usually observed for open framework materials, VSB-1 exhibits a layer type growth involving two types of building units. The presence of defects is closely related to both the building units and the growth mechanism. The units of growth, which are cages structure in this case, can accommodate new structural environments and produce new type of growth from the sites. Further studies linked to the way of synthesis, the use of surfactant, would help to understand better the relation between crystal growth and defect density. Indeed, the role of surfactant is important in porous materials. Changing it could drastically modify connections between atoms modifying the crystal growth and thus the pores. These factors are very important, especially those modifying the rate of defects in this material, which could drastically change the different properties obtained.

Acknowledgment

Financial supports from Japan Science and Technology Agency (JST), the Swedish Research Council (VR) and the Wallenberg Foundation are acknowledged.

References

[1] H. Sainte Claire Deville, C. R. Hebd. Seances Acad. Sci. 54 (1862) 324.
[2] W.M. Meier, D.H. Olse, C. Baerlocher, Atlas of Zeolite Structure Rypes, Elsevier, London, 1996.
[3] A.K. Cheetham, G. Férey, T. Loiseau, Angew. Chem Int. Ed. 38 (1999) 3268–3292.
[4] A.K. Cheetham, Science 264 (1994) 794.
[5] J.B. Parise, J. Chem. Soc. Chem. Commun. (1990) 1553.
[6] C.L. Cahill, Y. Ko, J.B. Parise, Chem. Mater. 10 (1998) 19.
[7] W. Schnick, J. Lücke, Angew. Chem. 104 (1992) 208.
[8] J.D. Martin, K.B. Greenwood, Angew. Chem. 109 (1997) 2162.
[9] J.L. Defreese, A. Katz, Micropor. Mesopor. Mater. 89 (2006) 25–32.
[10] M.W. Anderson, J.R. Agger, N. Hanif, O. Terasaki, T. Ohsuna, Solid State Sci. 3 (2001) 809–819.
[11] M.W. Anderson, J.R. Agger, N. Hanif, O. Terasaki, Micropor. Mesopor. Mater. 48 (2001) 1–9.
[12] I. Diaz, E. Kokkoli, O. Terasaki, M. Tsapatsis, Chem. Mater. 16 (2004) 5226–5232.
[13] T. Ohsuna, Y. Horikawa, K. Hiraga, O. Terasaki, Chem. Mater. 10 (1998) 688–691.
[14] V. Alfredsson, T. Ohsuna, O. Terasaki, J.O. Bovin, Angew. Chem Int. Ed. Engl. 32 (1993) 1210–1213.
[15] B. Slater, C.R.A. Catlow, Z. Liu, T. Ohsuna, O. Terasaki, M.A. Camblor, Angew. Chem Int. Ed. Engl. 41 (2002) 1235–1237.
[16] N. Guillou, Q. Gao, M. Nogues, R.E. Morris, M. Hervieu, G. Ferey, A.K. Cheetham, C. R. Acad. Sci. Paris 2 (1999) 387.
[17] X. Wang, Q. Gao, Mater. Lett. 59 (2005) 446–449.
[18] L. Xie, Q. Gao, X. Su, P. Wang, J. Shi, Micropor. Mesopor. Mater. 75 (2004) 135–141.
[19] J.-S. Chang, D.S. Kim, S.-E. Park, P.M. Forster, A.K. Cheetham, G. Ferey, Surf. Sci. Catal. 135 (2001) 3440–3447.
[20] P.M. Forster, J. Eckert, J.S. Chang, E.S. Park, G. Férey, A.K. Cheetham, J. Am. Chem. Soc. 125 (2003) 1309–1312.
[21] B. Schwenzer, K.M. Roth, J.R. Gomm, M. Murr, D.E. Morse, J. Mater. Chem. 16 (2006) 401–407.
[22] J.R. Agger, N. Hanif, C.S. Cundy, A.P. Wade, S. Dennison, P.A. Rawlinson, M.W. Anderson, J. Am. Chem. Soc. 125 (2003) 830–839.
[23] O. Terasaki, T. Ohsuna, Topics in Catalysis 24 (2003) 13–18.